

1 **Carbon emission reduction requires attention to the contribution of natural gas use:**
2 **Combustion and leakage**

3 Haoyuan Chen^{1,5}, Tao Song^{1,5*}, Xiaodong Chen², Yinghong Wang¹, Mengtian Cheng¹, Kai
4 Wang¹, Fuxin Liu⁴, Baoxian Liu³, Guiqian Tang^{1,5*}, Yuesi Wang^{1,5}

5 Correspondence to Guiqian Tang (tgq@dq.cern.ac.cn) Tao Song (st@dq.cern.ac.cn)

6 1. Key Laboratory of Atmospheric Environment and Extreme Meteorology, Institute of
7 Atmospheric Physics, Chinese Academy of Sciences, Beijing, China

8 2. Beijing Aozuo Ecological Instrument Co., Ltd., Beijing 100080, China

9 3. Beijing Key Laboratory of Airborne Particulate Matter Monitoring Technology, Beijing
10 Municipal Environmental Monitoring Center, Beijing, 100048, China

11 4. Anhui University of Science and Technology, Anhui 232001, China

12 5. University of Chinese Academy of Sciences, Beijing 100049, China

13 Abstract: Natural gas will continue to replace coal in the process of global energy structure reform,
14 but its leakage potential can delay the realization of global carbon neutrality. To quantify its impact,
15 we established a carbon dioxide (CO₂) and methane (CH₄) flux detection platform on the 220-m
16 platform of the Institute of Atmospheric Physics, Chinese Academy of Sciences, located in
17 northwestern Beijing. The observation results indicated that the daily mean CO₂ and CH₄ fluxes
18 were $12.21 \pm 1.75 \text{ } \mu\text{mol} \cdot \text{m}^{-2} \cdot \text{s}^{-1}$ and $95.54 \pm 18.92 \text{ } \text{nmol} \cdot \text{m}^{-2} \cdot \text{s}^{-1}$, respectively. The fluxes were
19 significantly correlated with natural gas consumption, indicating that natural gas has become a
20 common source of CH₄ and CO₂, the combustion of which releases CO₂, while its leakage processes
21 emit CH₄. Vehicle-based identification demonstrated that CH₄ can escape at the production, storage
22 and use stages of natural gas. Based on natural gas consumption data, the upper limit of the
23 calculated natural gas leakage rate in Beijing reached $1.12\% \pm 0.22\%$, indicating that the
24 contribution of CH₄ to climate change could reach 23 % of that of CO₂ on a 20-year scale. Natural
25 gas leakage was estimated to delay the time for China to achieve carbon neutrality by at least almost
26 four years.

27 **KEY WORDS:**

28 CO₂ flux, CH₄ flux, Eddy covariance, Natural gas leakage, Climate forcing, Carbon neutrality

29 **1. INTRODUCTION**

30 In 2015, the 1.5 °C temperature control target was proposed in the Paris Agreement to reduce

31 the occurrence of extreme weather events(Seneviratne et al., 2018). To achieve this goal, it is
32 necessary to actively promote the low-carbon development transformation of the economic system,
33 especially energy transformation. In this process, natural gas plays an important role, and typical
34 countries have indicated a trend of coal reduction and gas increase during energy structure
35 adjustment over the past century. It is expected that global natural gas consumption will continue to
36 increase by 2035.

37 Natural gas is commonly referred to as a clean alternative to coal, but its main component is
38 methane, with a global warming potential (GWP) that is 29.8 times greater than that of carbon
39 dioxide at the hundred-year scale(Environmental-Protection-Agency, 2024). If 3.4 % of methane
40 leaks into the atmosphere before natural gas combustion, the advantages of natural gas over coal
41 will become negligible(Kemfert et al., 2022). Recent studies have suggested that the average loss
42 rate of natural gas in cities worldwide ranges from 3.3 % to 4.7 %(Sargent et al., 2021). According
43 to statistics from the International Energy Agency (www.iea.org) in 2020, methane leakage in the
44 global oil and gas industry reached 72 million tons and amounted to 6 billion tons of carbon dioxide
45 equivalent (CO₂e) within 20 years. Therefore, it is unclear whether natural gas can become a
46 bridging material for energy transformation.

47 One important prerequisite is to determine the contribution of natural gas leakage during coal-
48 to-gas conversion to urban methane (CH₄) emissions and its climate effects. At present, conventional
49 CH₄ monitoring methods include ground, aviation, and satellite monitoring methods. Ground
50 monitoring aims to detect the atmospheric CH₄ concentration through the installation of sensors and
51 monitoring stations at fixed locations or on vehicles(Wunch et al., 2016). Notably, monitoring
52 equipment is often installed near potential emission sources, with high detection accuracy but
53 generally a limited spatial range. The aviation monitoring method can be employed to identify large-
54 scale CH₄ emissions through measurement techniques such as drones or aircraft but cannot be used
55 to achieve long-term monitoring(Duren et al., 2019; Frankenberg et al., 2016; Sherwin et al., 2024).
56 Satellite methods can compensate for the shortcomings of the former two methods(Chen et al., 2022;
57 Cusworth et al., 2018; Shen et al., 2023), which exhibit interference from clouds and require
58 significant labor and financial investments.

59 The eddy covariance method, which is based on tall towers, enables long-term monitoring of
60 methane emissions, thus facilitating the identification of methane sources in specific areas. However,

61 it should be noted that this method has certain limitations during urban flux measurements at higher
62 altitudes, as larger air volumes in the measurement system may lead to a significant imbalance
63 between the observed vertical turbulence exchange and surface net flux compared with those at
64 typical measurement heights. However, this deficiency should be considered in conjunction with
65 the advantages of urban tower measurements because cities typically correspond to deeper rough
66 sublayers that can extend to 2–5 times the average building height(Barlow, 2014). Therefore,
67 increasing the measurement altitude can help characterize the turbulent exchange between this layer
68 and the inertial sublayer.

69 Developing countries are the main driving force behind the continuous growth in global energy
70 demand. As Beijing is the capital of the world's largest developing country and the first city within
71 China to complete the coal-to-gas conversion process, clarifying the natural gas leakage process in
72 Beijing can provide guidance for energy transformation in developing countries regionally and even
73 globally. In this study, three aspects related to natural gas were investigated as follows. First, the
74 fluxes of CH₄ and CO₂ were observed simultaneously via the eddy covariance method, which was
75 used to investigate the impact of the coal-to-gas policy on CO₂ and CH₄ in Beijing, including the
76 magnitude of CO₂ emission and the common effects on the sources of both. Second, with navigation
77 experiments, the natural gas leakage process in Beijing has been confirmed, and the emission levels
78 of natural gas at different stages have been further roughly estimated, which provides certain
79 effective insights for the control of natural gas leakage in Beijing. Third, we discuss climate forcing
80 caused by natural gas leakage while considering the CO₂ flux as a basis, calculate the natural gas
81 leakage rate with statistical data, and estimate the impact of natural gas leakage on China's carbon
82 peak and carbon neutrality in conjunction with existing reports.

83

84 **2. METHODS**

85 **2.1 Instrument setup for eddy covariance measurement**

86 The measurements were conducted at a 325-m high meteorological tower in northwestern
87 Beijing, with a closed-path observation system installed on a platform at a height of 220 m, which
88 included a dual laser gas analyzer (QC-TILDAS-DUAL, Aerodyne Research Inc., USA), three-
89 dimensional ultrasonic anemometer (Gill Instruments, Ltd., Lymington, Hampshire, UK), vacuum
90 pump (XDS35i, BOC Edwards, UK), data collector (CR6, Campbell Scientific Inc., USA), and

91 other accessories. In the dual laser gas analyzer, tunable infrared laser direct absorption spectroscopy
92 (TILDAS) technology is used to detect the most significant fingerprint transition frequencies of
93 molecules within the mid-infrared wavelength range. The analyzer has an optical path of up to 76
94 m and can measure H₂O, CO₂ and CH₄ simultaneously. Similar instruments have been applied to
95 observe outdoor ecosystems(Zöll et al., 2016). Under the action of a vacuum pump, the air sample
96 enters the instrument room at a flow rate of 2 lpm through a polytetrafluoroethylene sampling tube
97 with a length of 3 m and an inner diameter of 3 mm (Figure S1). Instrument calibration includes
98 zero-point and range calibration processes. High-purity nitrogen gas (>99.999 %) was used for zero-
99 point calibration at 1-hour intervals. In this process, the corresponding solenoid valve was opened,
100 which was automatically controlled by TDLWintel software, and range calibration was performed
101 at the factory. In addition, before the experiment, we calibrated the gas analyzer using CO₂ (401
102 ppm) and CH₄ (2190 ppb) standard gases. We found that the measured and standard gas
103 concentrations differed by less than 1 %, indicating satisfactory instrument performance. Therefore,
104 we did not perform range calibration later. The instrument was placed in an insulated box equipped
105 with air conditioning to ensure normal operation of the laser. Both instruments were operated at a
106 sampling frequency of 10 Hz. The data collector and high-frequency instrument were timed
107 according to the network and global positioning system (GPS), respectively, to maintain
108 synchronization. To minimize the twisting effect of the flux tower on the incoming air, a three-
109 dimensional ultrasonic anemometer was installed at the end of a 1.5-m long support arm facing
110 southeast China in summer. This measurement lasted from June 11 to September 7, 2022, during
111 which the nitrogen cylinder was replaced, and the instrument was debugged on June 18 and 19.
112 From July 12 to 26, the experiment was stopped due to failure of the tower power supply.

113 **2.2 Flux data processing**

114 The flux data processing operation in this study is based on the eddy covariance technique via
115 EddyPro software (version 6.2.1, Li COR, Inc.; Lincoln, Nebraska, USA). An average flux
116 calculation period of 30 minutes was selected(Lee, 2004). Before calculating half-hourly fluxes,
117 spike detection and data rejection algorithms were applied like follows as described by Vickers et
118 al., (1997): Take a moving window with a width equal to 1/6 of the averaging period (typically 5
119 minutes) and calculate the mean and standard deviation of the time series within the window. Define
120 outliers as any data points deviating from the mean by n times the standard deviation (initial n =

121 3.5). Replace the identified outliers with linearly interpolated values from adjacent points.
122 Consecutive outliers ≤ 3 are treated as a single outlier; consecutive outliers ≥ 4 are considered local
123 trends and excluded from outlier classification. Iteratively increase n by 0.1 per cycle until no
124 outliers are detected or 20 iterations are reached. Advance the window by half its width (step size)
125 and repeat outlier detection/removal for the next window. Continue this process until all outliers are
126 processed within the averaging period. If outliers exceed 1 % of the total data points in any averaging
127 period, discard that entire period.

128 The double rotation method proposed by Kaimal et al., (1994) was employed for tilt correction.
129 The delay time caused by the spatial separation of gas analyzers and three-dimensional ultrasonic
130 anemometers (as well as the injection pipeline of closed-path systems) was corrected via the
131 maximum covariance method(Fan et al., 2012). Webb, Pearman, and Leuning (WPL) correction
132 was not applied here(Webb et al., 2007) because the instrument room was in a state of constant
133 temperature and pressure that converted the real-time concentration into a dry volume mixing ratio,
134 and the longer pipeline of the closed-path system avoided the influence of temperature fluctuations.
135 The limitations of eddy covariance systems can lead to frequency loss in flux observations. Factors
136 such as a limited average period and linear detrending can cause low-frequency loss, whereas
137 instrument separation, path averaging, insufficient high-frequency responses, and pipeline
138 attenuation can cause high-frequency loss. The method proposed by Moncrieff et al., (1996) was
139 employed for frequency response correction. After the above correction of the flux data, in this paper,
140 the 0-1-2 quality labeling scheme proposed by Mauder and Foken(Mauder et al., 2004) was adopted
141 for data quality control purposes. Notably, a value of 0 represents data with the best quality, a value
142 of 1 represents data with good quality, and a value of 2 represents data with poor quality. In this
143 study, flux data marked as 2 were excluded from the subsequent analysis. In addition, the flux source
144 area was evaluated via the method of Kljun et al., (2004) (Text. S1), and the flux source area covered
145 most of the urban area of Beijing and reflected the average emission characteristics of urban Beijing
146 (Figure S2).

147 **2.3 Spectral analysis**

148 High-frequency signal loss can occur in closed-path systems. To determine the response
149 capability of the closed-path system to high-frequency turbulence signals, we analyzed the observed
150 gas exchange signals through the turbulence power spectrum. The selected time ranges from 12:00

151 to 16:00 every day during the observation period, with a total of 8 and a half hours of data. The data
152 were integrated and averaged, and the data curve was then compared with the ideal slope in the
153 inertia subarea (Figure S3). $Co(wT)$ followed the theoretical $f_n^{-4/3}$ (where f_n denotes the normalized
154 frequency) in the inertial subregion. In contrast, the slopes of $Co(wCO_2)$ and $Co(wCH_4)$ were
155 slightly greater than $-4/3$, indicating that there was high-frequency loss in the flux observations of
156 the closed-loop system(Kaimal et al., 1972). Through high-frequency correction, the calculation
157 results indicated that the CO_2 and CH_4 fluxes were 7.73 % and 6.85 % greater, respectively, than
158 those before correction.

159 **2.4 Mobile CH_4 and CO_2 observations**

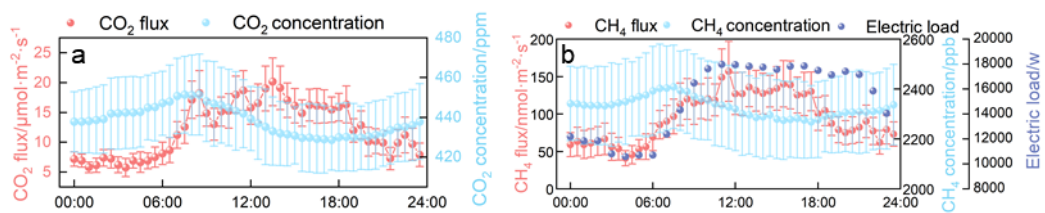
160 Vehicle-based experiments were conducted in the urban area of Beijing in the winter of 2023
161 and the summer of 2024, and the specific deployment of the mobile observation station is shown in
162 Figure S1. Notably, the car was equipped with a CO_2/CH_4 spectrometer (Los Gatos Research, Inc.,
163 USA), a laptop for data viewing, and a mobile power supply (Figure S4). Zero-point calibration of
164 the instrument was performed once pure nitrogen was used before the mobile experiment began.
165 Standard gases of methane and carbon dioxide were introduced to calibrate the instrument
166 simultaneously, and we found that the concentration of the instrument matched well with the
167 standard gas. Since we focused more on the enhancement in concentration rather than itself, we did
168 not calibrate it again afterward. The sampling port was located approximately 20 cm from the roof,
169 and ambient air was collected through a PTFE tube with a length of 2 m and an inner diameter of 3
170 mm. Before the particulate matter entered the instrument, it was removed using a filter head. The
171 IMET sounding instrument (International Met Systems, USA) is installed on the roof, with a
172 sampling frequency that is consistent with that of the other instruments, i.e., 1 s, real-time
173 concentration information of different latitudes and longitudes is obtained at a resolution of seconds
174 through the corresponding time between the GPS and the instrument; for example, if the GPS
175 sampling time delay is 3 s, the latitude and longitude coordinates are reassigned to the CH_4 reading
176 observed three seconds prior. Our observation sites include petrochemical plants located in
177 southwestern Beijing, natural gas storage tanks and landfills in the northeastern part, and power
178 plants with the highest natural gas usage in the southeastern part.

179 **3. RESULTS**

180 **3.1 Diurnal variation in the flux**

181 A positive or negative flux reflects the vertical exchange direction of trace gases in the urban
182 canopy, which is positive upward and negative downward. (The uncertainty analysis is described in
183 the Text. S2 and Figure S5, respectively) Overall, both CO₂ and CH₄ fluxes are positive on a daily
184 scale, indicating that cities are the source of both gases. The diurnal CO₂ flux ranged from 6.05 to
185 19.66 $\mu\text{mol}\cdot\text{m}^{-2}\cdot\text{s}^{-1}$ with an average of $12.21 \pm 1.75 \mu\text{mol}\cdot\text{m}^{-2}\cdot\text{s}^{-1}$ (Figure 1a), which was generally
186 lower than the summer observations by Cheng et al., (2018) and Liu et al., (2012) at 200 m and 140
187 m at this tower, respectively (Table S1), a smaller deviation suggests that CO₂ may be dominated
188 by a more stable source than before. We also obtained observation results at 140 m in summer from
189 2009–2017 (Liu et al., 2020). The flux in 2022 significantly decreased compared with previous
190 levels (Figure S6), which reflects the transformation of Beijing's energy structure. The coal-to-gas
191 policy implemented by Beijing these years led to a gradual decrease in the proportion of coal in
192 primary energy consumption, with a steady increase in the proportion of natural gas in total
193 consumption (Figure S7), the use of natural gas results in much less coal CO₂ than coal, generating
194 the same amount of heat; moreover, Beijing has increased the amount of electricity flow from other
195 provinces in recent years (Figure S7), which has further driven a decrease in the annual average
196 concentration of PM_{2.5}, dropping to 30.5 $\mu\text{g}\cdot\text{m}^{-3}$ by 2024. In fact, previous studies have reported a
197 high correlation between PM_{2.5} and CO₂ fluxes. For example, Donato et al., (2019) found that the
198 seasonal and daily variations in the particle number flux in southern Italian suburbs are largely
199 determined by both transportation activities and household heating. Liu et al., (2020) confirmed that
200 the CO₂ flux can explain 64 % of the interannual variation in the PM_{2.5} concentration by fitting the
201 correlation between the annual average PM_{2.5} and CO₂ fluxes in Beijing from 2009 to 2017.
202 Therefore, controlling CO₂ emissions can also greatly control the concentration level of PM_{2.5},
203 thereby achieving the dual effects of mitigating climate change and improving air quality. In terms
204 of its diurnal variation, it did not follow a typical bimodal pattern but rather remained high after
205 reaching the first peak at 8:00, with a lower level at night, reflecting high anthropogenic carbon
206 emissions during the day, such as those resulting from transportation and energy generation
207 activities. The diurnal pattern of the CH₄ flux was similar to the observation results of Giolo et al.,
208 (2012) and Helfer et al., (2016) (Figure 1b), reflecting an increase in emissions during the day. The
209 CH₄ flux began to increase gradually from 04:00 to around 08:30, and then remained stable until

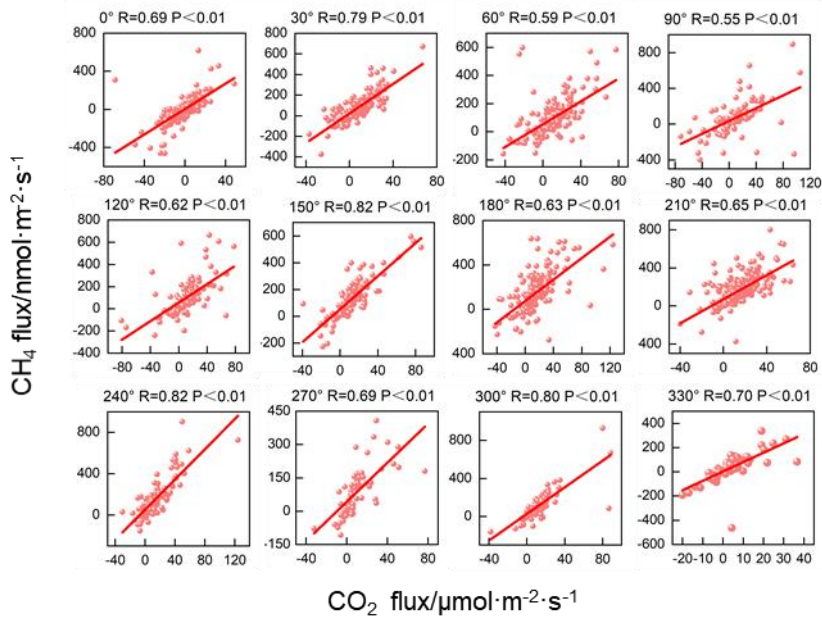
210 after 10:30, when it began to rise rapidly again, reaching its daily peak of approximately 157.1 nmol
 211 $\text{m}^{-2} \text{ s}^{-1}$ around 11:30. After 17:30, it slowly declined. Its diurnal variation pattern showed some
 212 differences compared to CO_2 flux, which increased beginning at 03:30 to around 08:30 similar to
 213 CH_4 flux. However, the peak for CO_2 flux occurred around 13:30, then slowly decreased and
 214 decreased rapidly after 18:30, Assuming that the average CH_4 flux at midnight (00:00 to 06:00) can
 215 be employed as the baseline for nighttime emissions, it accounted for 58 % of the daily average flux.
 216 The CH_4 flux demonstrated a pronounced diurnal pattern, indicating a significant daily variation in
 217 the background source in the source area.



218
 219 Figure 1 Daily variations in the CO_2 and CH_4 concentrations, fluxes, and electricity loads

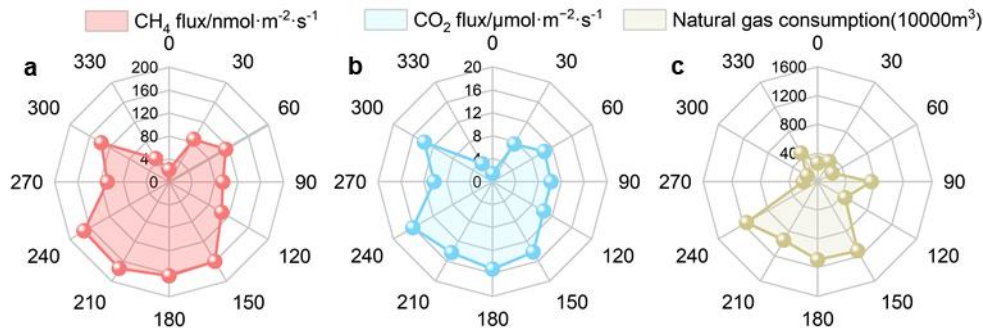
220 3.2 Homology between CO_2 and CH_4

221 The CO_2 and CH_4 fluxes showed a significant correlation along all directions (Figure 2), with
 222 correlation coefficients greater than that at the center of Loz, Poland (0.50)(Pawlak et al., 2016), but
 223 the low correlation between the CO_2 and CH_4 fluxes and the temperature excludes the conclusion
 224 that biological sources dominate their emissions (Figure S8). Therefore, CO_2 and CH_4 share the
 225 same anthropogenic sources within the source area. This homology is also reflected in their spatial
 226 distributions, with high fluxes distributed mainly south of the tower, which is more densely
 227 populated and encompasses complex industrial structures, and much lower fluxes in the northern
 228 forest and park areas (Figure 3a, b). The correlation between the spatial distributions of the CO_2 and
 229 CH_4 fluxes reached 0.98, demonstrating the common impact of similar anthropogenic sources on
 230 their emissions. The linear fitting results at 150° and 240° indicated the highest correlation
 231 coefficient (0.82) along all directions (Figure 2), further supporting this viewpoint.



232

233 Figure 2 Linear fitting results for the 30-minute CH_4 and CO_2 fluxes in the 12 directions



234

235 Figure 3 Mean CH_4 and CO_2 concentrations, fluxes and natural gas consumption in the 12
236 directions

237 4. DISCUSSION

238 4.1 Driver of the homology between CO_2 and CH_4

239 After the introduction of natural gas in 1985, the proportion of natural gas in the fossil
240 fuel industry of Beijing increased annually, especially when coal was replaced with natural gas
241 and electricity in 2014 and 2018, respectively, and natural gas became the most consumed f
242 ossil fuel (Figure 6a). According to the 2022 Beijing Statistical Yearbook (in Chinese; <https://nj.tjj.beijing.gov.cn/nj/main/2023-tnj/zk/e/indexch.htm>), natural gas is used mainly for thermal
243 power generation and heating (accounting for 69 %). Owing to the low proportion of heatin
244 g in summer, natural gas in Beijing is mostly used for thermal power generation in summer.
245 Owing to the difficulty in obtaining hourly electricity generation data, we obtained a daily va

247 riation curve of the electricity load in Beijing based on the statistical data (power plants usu
248 ally calculate the required electricity generation based on the electricity load) (source: Nation
249 al Energy Administration, China; <https://www.gov.cn/xinwen/2019-12/30/5465088/files/e3682ce168c8427b886a43a790d66c2c.pdf>) (Figure 1b). The daily variation in the electricity load is hi
250 ghly consistent with that in the CH₄ flux, with the maximum CH₄ flux occurring at 11:00 pm
251 during the peak electricity consumption period. After 16:00 pm, the electricity load and CH₄
252 flux decrease synchronously. Thus, the daily variation in the CH₄ flux is driven by natural g
253 as consumption. We gridded the natural gas consumption data (Figure S9) and calculated the
254 mean natural gas consumption along all directions within the flux source area (Figure 3c).
255 Notably, a high consistency between the spatial distributions of the CO₂ and CH₄ fluxes and
256 natural gas consumption was found, which reflects that after the adjustment of the energy str
257 ucture in Beijing, natural gas became the main source of CO₂ and CH₄. Considering the high
258 photosynthetic absorption of CO₂ by plants in summer, this conclusion also applies to the ot
259 her seasons, which supports the hypothesis that natural gas is the main source of winter CO₂
260 emissions in Beijing, as determined based on the isotope tracing method(Wang et al., 2022;
261 Wang et al., 2022).

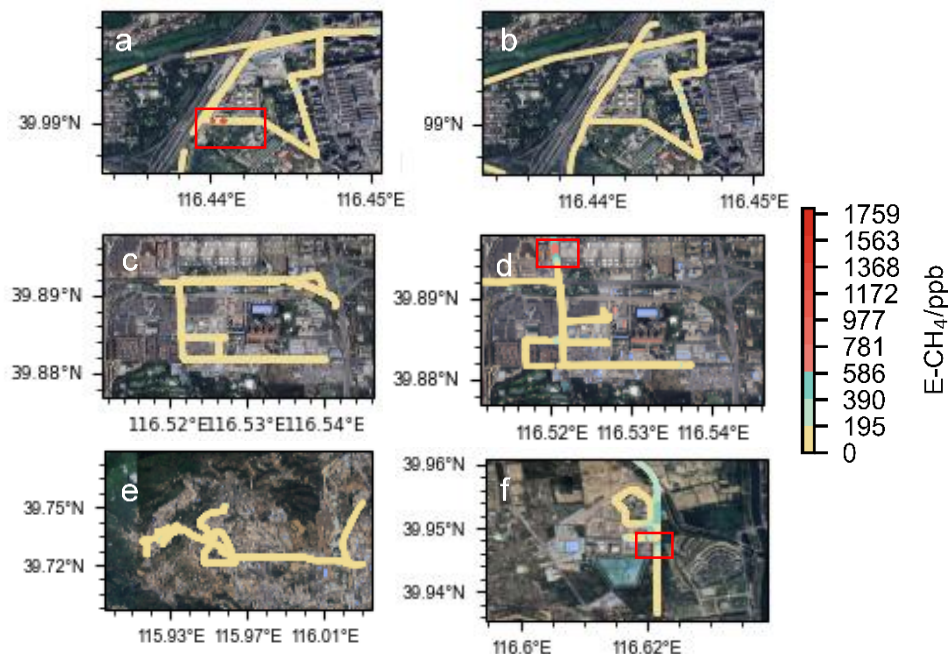
263 To verify this conclusion and identify the primary phases of natural gas leakage, we conducted
264 mobile observations during winter and summer around large petrochemical plants, gas storage tanks,
265 and power plants in Beijing. Given real-time variations in gas concentrations influenced by
266 meteorological conditions and pollution transport, it was essential to determine background
267 concentrations at each time point. The current mainstream approach for determining background
268 values involves calculating the 5th or 10th percentile within a sliding window of 5 minutes (± 2.5
269 min) or 10 minutes (± 5 min) centered on the target timestamp (Pu et al., 2023, Well et al., 2018;
270 Well et al., 2019). We compared and evaluated the results applying different combinations of time
271 windows or percentile following the method of Schiferl et al., (2025). (Text. S3). The 10-min time
272 window with 5th percentile was used here to calculate the background value. The enhancement
273 concentration can be defined as the difference between the observed value and the background value
274 at the corresponding time. There was significant CH₄ leakage around the gas storage tanks and
275 power plants in both winter and summer. Notably, the observed CH₄ hotspots were located in the
276 downzone of potential leakage sources; therefore, we attribute the high CH₄ concentration to the

277 emissions of these potential natural gas leakage sources. In winter, hotspots with concentrations
278 higher than the background value of 1759 ppb appeared around the gas storage tank (Figure 4a),
279 corresponding to an enhancement concentration of CH₄ (E-CH₄) and enhancement concentration of
280 CO₂ (E-CO₂) fingerprint line with a slope of 0.11 (Figure 5a). In addition, the enhancement
281 concentration fingerprint slopes of the other hotspot zones were 0.06 and 0.07, respectively,
282 indicating varying degrees of leakage around the gas storage tank(Sun et al., 2019).The
283 enhancement concentration fingerprint in summer also revealed leakage related to gas storage
284 equipment (Figure 4b), with a slope of 0.04, analogous to that of 0.06 in winter. Similar to gas
285 storage tanks, natural gas leakage hotspots have been observed in various equipment in power plants.
286 For example, fingerprints with a slope of 0.005 (Figure 5d) in summer reflected leakage related to
287 combustion devices or pipeline in power plants(Lamb et al., 1995), whereas fingerprints with a slope
288 of 0.015, 0.02 or 0.05 reflected leakage related to storage facilities (Figure 5c,d)(Hurry et al., 2016).
289 We also discovered natural gas leakage near the petrochemical plant (Figure 4e), the line with a
290 slope of 0.02 was related to the gas storage equipment, and the line with a slope of 0.005 was
291 relevant to the natural gas combustion equipment. As important sources of methane, landfills have
292 received widespread attention, so we also conducted mobile observations near a large landfill
293 outside the Fifth Ring Road in Beijing, which was a hotspot exhibiting a level exceeding the
294 minimum concentration of 1375 ppb (Figure 4f). The concentration fingerprints were relatively
295 disordered and significantly differed from those of CH₄ emissions dominated by natural gas (Figure
296 5f), indicating that waste disposal processes are relatively complex and cannot be ignored in
297 cities(Cusworth et al., 2024).

298 Converting observed concentration increments into emission rates is a simple means of
299 quantifying natural gas leakage, which is subject to atmospheric conditions and potential leak source
300 locations. Weller et al., (2018; 2019) developed a model based on the relationship between the
301 enhancement concentration and emission rate. The specific formula is shown in Text S4. The model
302 assumes that CH₄ enhancement is the best predictor of the leakage emission rate and that a greater
303 leakage emission rate corresponds to greater CH₄ enhancement. The method sets a minimum
304 threshold for the observed CH₄ concentration, which is 110 % of the background value, to filter out
305 concentration changes caused by measurement. Moreover, when multiple detections are conducted
306 for the same leakage source, it is necessary to average the CH₄ enhancement values and then

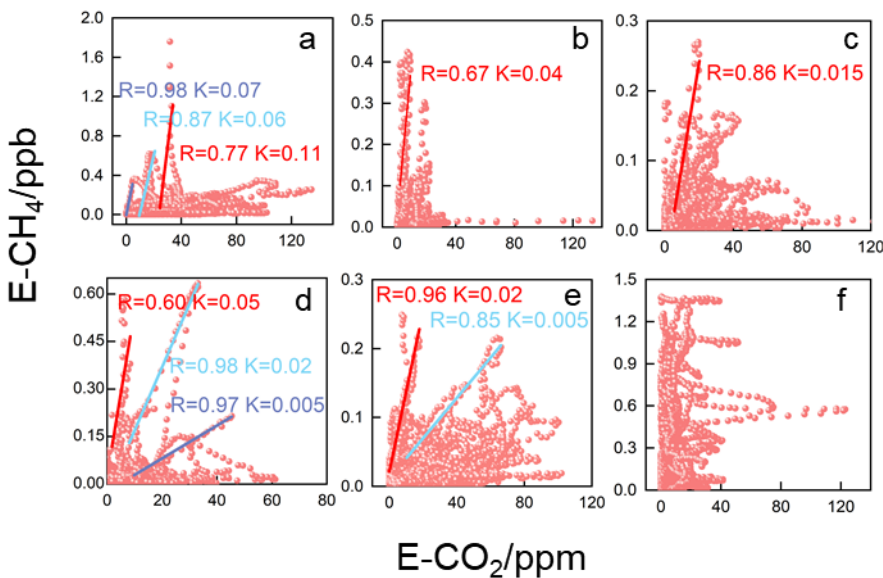
307 substitute them into the above formula. We estimated the natural gas leakage emission rates from
 308 different leakage sources with this method, and the confidence interval (CI) based on the Bootstrap
 309 method was used to estimate the uncertainty of the leakage rate. The natural gas leakage rate from
 310 the gas storage tank and power plant in winter were 7.4 ± 0.1 g/min and 0.6 ± 0.03 g/min,
 311 respectively, and the natural gas leakage rate from the gas storage tank and power plant in summer
 312 were 1.2 ± 0.04 g/min and 2.1 ± 0.07 g/min, respectively. The natural gas leakage rate near the
 313 petrochemical plant was 0.6 ± 0.04 g/min, which was lower than the results of Ars et al., (2020) on
 314 the leakage rates of Toronto's natural gas distribution network (3.5–10.6 g/min), but they noted that
 315 Well's method underestimated the leakage rate because it ignored smaller concentration
 316 enhancements. A significant uncertainty in this method lies in the distance between the leakage point
 317 and the vehicle; unfortunately, determining the distance between the two points in practical
 318 operation is difficult, which may confound the estimation of methane leakage. Therefore, sufficient
 319 mobile experiments should be conducted in subsequent work to accurately calculate natural gas
 320 leakage in Beijing.

321



322

323 Figure 4 CH₄ enhancement concentration distribution map based on vehicle observations (a, c
 324 show storage tanks and thermal power plants in winter; b, d show storage tanks and thermal power
 325 plants in summer; e shows petrochemical plants; f shows waste disposal station; and the red box
 326 represents high leakage value, The background image is from Google Earth (© Google Earth))



327

328 Figure 5 Fitting of the CO₂ and CH₄ concentration enhancement values (a, c show the fitting
 329 results for the gas storage tanks and power plants in winter; b, d show the fitting results for the gas
 330 storage tanks and power plants in summer; e shows the petrochemical plants; and f shows the
 331 waste disposal stations. Different fitting lines represent various leakage sources.)

332 **4.2 Climatic effects of natural gas (NG) losses and their impact on carbon neutrality**

333 Based on the natural gas consumption and flux data for the flux source area, the estimated
 334 upper limit of the natural gas leakage rate in Beijing reached 1.12 % \pm 0.22 % (Text. S5), and the
 335 lower limit of natural gas leakage in Beijing was estimated to be 0.82 % considering the emissions
 336 from biogenic sources (Text. S6). If the CH₄ fluxes were attributable solely to pipeline leakage
 337 processes, the CH₄ fluxes should remain relatively stable throughout the day without significant
 338 diurnal variations, given the constant pressure in urban pipeline pressures. However, in our
 339 observations, the CH₄ fluxes exhibited pronounced diurnal patterns and their spatial distribution
 340 positively correlated with natural gas consumption. This indicates that CH₄ emissions in Beijing
 341 originate predominantly from consumption-oriented leakage processes. Consequently, as natural
 342 gas consumption surges during winter heating periods, CH₄ emissions from these processes (e.g.,
 343 fugitive emissions from electrical devices) also increase. As a result, the ratio of emissions to
 344 consumption (leakage rate) remains relatively stable. Thus, the CH₄ leakage rate measured in
 345 summer is representative of year-round leakage rate of natural gas.

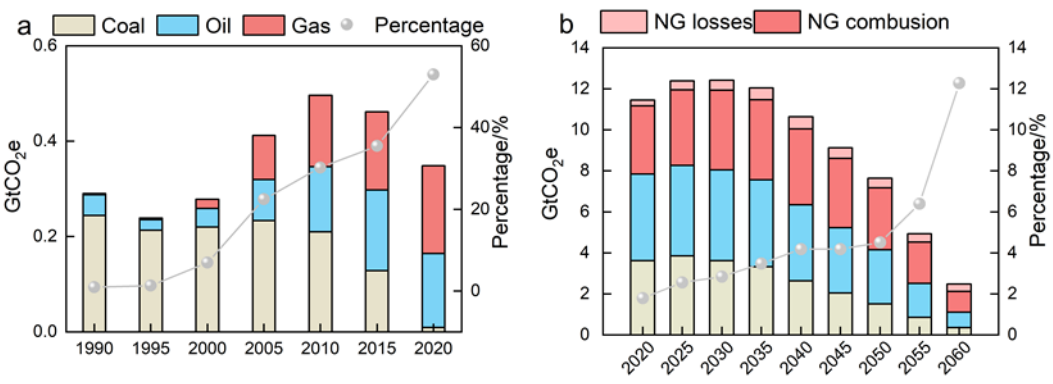
346 Our measured leakage rate was lower than the value of 2.07 % calculated based on the purchase
 347 and sales statistics and the statistical mean value of 1.1 %–1.65 % reported by the American

348 Petroleum Institute (<https://www.api.org/>). Nevertheless, the contributions of CH₄ to climate
349 warming are 8.37 % and 23.17 % of those of CO₂ at the 100- and 20-year scales, respectively,
350 according to the determined CO₂ and CH₄ fluxes and the GWP of CH₄. With the arrival of the winter
351 heating season, climate forcing will further increase on a yearly scale. Assuming that the natural gas
352 consumption in Beijing during the heating season is 5 times greater than that during the other
353 seasons (according to Beijing Gas in 2019), that oil consumption does not significantly fluctuate
354 throughout the year and that both the CO₂ and CH₄ fluxes are positively correlated with fossil fuel
355 consumption and natural gas leakage, the climate forcing effect of natural gas leakage in 2022 was
356 11.47 % on a 100-year scale and could reach as high as 31.56 % on a 20-year scale. However, when
357 the same amount of heat is generated, the use of natural gas could yield CO₂ emission reductions of
358 50 % relative to coal and of only approximately 30 % relative to oil. Therefore, the reduction in
359 greenhouse gas emissions resulting from natural gas combustion compared with that resulting from
360 the combustion of other fossil fuels may be offset by the climate forcing effect of CH₄ leakage in
361 the short term, making it difficult for natural gas to become a transitional energy source for energy
362 transition.

363 To assess the impact of natural gas leakage on carbon peak and carbon neutrality bas
364 ed on our quantified leakage rate, scaling the Beijing-derived leakage rate to a national le
365 vel is needed. However, due to the absence of leakage rate data from other cities, we can
366 provide only a rough estimate based on available data as follows: according to the 14th
367 Five-Year Plan for National Urban Infrastructure Development (in Chinese; <https://www.go>
368 v.cn/zhengce/zhengceku/2022-07/31/5703690/files/d4ebd608827e41138701d06fe6133cdb.pdf), c
369 ities in China are divided into three categories—major cities (natural gas penetration rate
370 $\geq 85\%$), medium cities (natural gas penetration rate $\geq 75\%$), and small cities (natural gas
371 penetration rate $\geq 60\%$). The China Gas Development Report 2023 (Economics & Develop
372 ment Research Institute of SINOPEC, 2023) further supplements pipeline coverage progres
373 s, indicating that large cities and developed regions (e.g., Beijing, the Yangtze River Delta,
374 the Pearl River Delta) accounted for approximately 30 %–40 % of the national pipeline 1
375 length in 2022, here set at 35 %. Small/medium cities constituted 60 %–70 % of the total
376 pipeline length, here set at 65 %. A study based on Bayesian network modeling revealed
377 that leakage probabilities in small/medium cities are 1.8 times higher than those in major

378 cities (95% CI: 1.6–2.0)(Gao et al., 2024). Consequently, the national leakage rate was cal
 379 culated as $1.7\% (95\% \text{ CI: } 1.57\%–1.85\%) = 0.35 \times 1.12\% + 0.65 \times 1.12\% \times 1.8 (95\% \text{ CI: } 1.$
 380 $6–2.0)$.

381 Then we adopted the results of the Global Climate Governance Strategy and China's Carbon
 382 Neutrality Path Outlook(Wang et al., 2021), which indicates that CO_2 emissions in China under the
 383 carbon neutrality scenario reach approximately 2.1 Gt. We calculated CH_4 leakage in the
 384 corresponding year based on the natural gas consumption level under the future scenario of the
 385 China Energy Outlook 2060 (SINOPEC 2021)(Economics-and-Development-Research-Institute,
 386 2021). All of the calculation results were converted CO_2 equivalents (CO_2e) according to the GWP
 387 on a 20-year scale (Figure 6b). After taking into account the natural gas leakage process, the CO_2e
 388 in China will still peak by 2030. However, the CO_2e resulting from natural gas leakage will reach
 389 0.37 Gt (95 % CI: 0.34 Gt–0.40 Gt) in 2060, compared to 0.26 Gt previously. This accounts for
 390 approximately 16.6 % (95 % CI: 15.4 %–17.9 %) of the total CO_2 emissions (excluding natural gas
 391 leakage) and 35.9 % (95 % CI: 33.2 %–38.8 %) of the total CO_2 emissions from natural gas
 392 combustion, which is comparable to the CO_2 emissions from coal combustion (0.35 Gt). Since
 393 natural carbon sinks do not show significant short-term fluctuations, the future increase in carbon
 394 sinks will mainly rely on carbon capture and storage (CCS) technology. Given the current estimated
 395 CO_2 capture rate of CCS technology (0.1 Gt/year, as estimated by the China Energy Outlook 2060
 396 (SINOPEC 2021)), the achievement of carbon neutrality in China will likely be delayed by nearly
 397 three to four years. Therefore, when determining future natural gas consumption levels, it is
 398 necessary to both consider the leakage effects of natural gas and utilize carbon modeling.



399
 400 Figure 6 Terminal consumption of coal, oil, and natural gas and their proportions from 1990 to
 401 2020(a) Since diesel-powered trucks are allowed only at night on the Fifth Ring Road and
 402 kerosene, which is used mainly in aviation and is not included in the flux source area, oil mainly

403 comprises gasoline in this case), CO₂ equivalent from coal, oil and natural gas (losses and
404 combustion) in the future scenario (estimated by China Energy Outlook 2060 released by
405 SINOPEC in 2021), and CO₂ equivalent of natural gas leakage as a proportion of natural gas (NG)
406 combustion emissions(b)

407 **4.3 Policy implications**

408 Our observations revealed a strong correlation between CH₄ emissions and natural gas
409 consumption in terms of both their daily variations and spatial distributions, that is to say, the
410 terminal consumption process drive natural gas leakage in Beijing. Liu et al., (2023) established a
411 bottom-up emission inventory and reported that the terminal use process in Beijing accounts for 80 %
412 of the total methane emissions in the entire natural gas supply chain. Therefore, the Chinese
413 government may need to expand the detection of pipeline leakage to the entire natural gas industry
414 chain.

415 Notably, existing grid-based inventory products also exhibit significant uncertainty in terms of
416 methane sources. The extracted inventory originates from the Emissions Database for Global
417 Atmospheric Research (EDGAR) (<https://edgar.jrc.ec.europa.eu/EDGARv8.0>). Although the mean
418 methane flux (126.3 nmol·m⁻²·s⁻¹) within the source area is close to our results, the terminal use
419 process accounts for only approximately 13 % of the annual methane emissions, suggesting that
420 many potential urban methane sources could have been missed, which should be considered in
421 inventory refinement in the future.

422 In addition, minimizing the methane leakage rate could ensure the early realization of carbon
423 neutrality in China. Although methane emission control has been included in the agenda for the first
424 time in the Methane Emission Control Action Plan promulgated in 2023, which clearly highlights
425 the need to promote the application of leak detection and repair technology and to enhance the
426 comprehensive recovery and utilization of methane, methane leakage standards have not been
427 updated. Previous methane leakage standards focused only on controlling the amount of methane
428 leakage from a safe perspective, thereby ignoring the climate effects of natural gas leakage. China
429 must urgently develop a strict and detailed set of natural gas leakage standards.

430 **4.4 Limitations**

431 The flux discussed in this study is net flux, which means considering both positive flux and
432 negative flux simultaneously. It should be noted that for flux values close to zero (particularly the
433 negative values observed at night), we have retained all the data points without employing a filtering

434 method based on the statistics of instrument white noise. Whereas a more rigorous approach would
435 be to model these fluxes fluctuating around zero as white noise and establish a statistical significance
436 threshold based on this. Discarding all values within this threshold (including slightly positive and
437 slightly negative ones) could effectively reduce noise-induced bias, although at the cost of data
438 coverage. The development and application of such objective, instrument-physics-based filtering
439 criteria represent an important direction for future research to enhance the quality and reliability of
440 flux data, particularly under low-turbulence conditions.

441 For the source analysis of CO₂ and CH₄, we did not consider the impact of long-distance
442 transportation. However, this impact may not be completely ignored. For example, in the upwind
443 area of Beijing, Shanxi Province is a high-intensity area of anthropogenic pollutant emissions, where
444 the actual lifespan of local CO may be significantly shortened due to the influence of local OH
445 concentration. The CO₂ produced by CO there is not insignificant (Li et al., 2025), which may also
446 be one of the sources of local CO₂ in Beijing. Therefore, it is necessary to combine regional chemical
447 transport models to more accurately quantify the impact of local chemical coupling in future flux
448 research.

449 When quantifying CH₄ leakage from different natural gas facilities, we adopted a quantile
450 based deterministic method to separate background concentration from enhanced signals, and
451 mainly explored the sensitivity brought by algorithm parameter selection. However, this framework
452 has a fundamental limitation: it fails to incorporate the inherent observational uncertainty of
453 background concentration and on-site observed concentration into a unified probabilistic analysis.
454 The observation error of background value and enhanced signal are coupled (Lu et al., 2025; Zheng
455 et al., 2025), they will propagate together, and significantly affect the final uncertainty interval of
456 emission estimation. Our current sensitivity analysis can only be one step in such comprehensive
457 uncertainty quantification work (i.e. identifying sensitivity to parameter selection), and future work
458 should focus on: (1) systematically quantifying the instrument errors used in this study; (2)
459 integrating these prior uncertainties into the inversion process of emissions using probabilistic
460 frameworks such as Bayesian inference or error propagation models; (3) expanding the emission
461 estimation from a single 'best estimate' to a probability distribution that includes confidence
462 intervals.

463 Although we estimated the impact of natural gas leaks on China's carbon neutrality process,

464 the national-scale extrapolation of the natural gas leakage rate conducted in this study carried
465 substantial uncertainty. Our approach, which relied on a simplified scaling method due to data
466 availability constraints, may fail to account for strong regional heterogeneities in natural gas
467 consumption patterns and infrastructure conditions. As highlighted by recent literatures (Qin et al.,
468 2023; Hu et al., 2024), such scaling methods can systematically miss substantial emission sources
469 in specific regions (e.g., industrial hubs like Shanxi Province). Therefore, our national estimate
470 should be interpreted as a rough attempt.

471 **5. Conclusions and outlooks**

472 This study utilized the eddy covariance method to measure CO₂ and CH₄ fluxes at 220-m height
473 in urban Beijing, providing critical insights into surface-atmosphere exchanges of greenhouse gases
474 in the region. First, urban areas unequivocally act as net sources of both CO₂ and CH₄. The daily
475 mean fluxes were $12.21 \pm 1.75 \text{ } \mu\text{mol} \cdot \text{m}^{-2} \cdot \text{s}^{-1}$ for CO₂ and $95.54 \pm 18.92 \text{ } \text{nmol} \cdot \text{m}^{-2} \cdot \text{s}^{-1}$ for CH₄, with
476 daytime emissions significantly exceeding nighttime levels, highlighting the importance of
477 anthropogenic influences.

478 Although diurnal variation patterns differed slightly between CO₂ and CH₄ fluxes, their strong
479 correlation indicates shared dominant sources. Spatial distribution analysis revealed high
480 consistency between both fluxes and natural gas consumption patterns, confirming natural gas as a
481 common source. With Beijing's energy restructuring, natural gas has become the dominated
482 terminal energy consumption. Its combustion releases substantial CO₂, while leakage processes emit
483 CH₄, as validated by mobile observations detecting CH₄ fugitive emissions during production,
484 storage and use stages. Although biogenic sources could contribute to CH₄ emissions, they account
485 for at most 27 % of total CH₄ fluxes in the source area, ruling out the view that biological sources
486 dominate both emissions. Attributing all CH₄ emissions to natural gas usage, the upper leakage rate
487 of natural gas in Beijing was calculated as $1.12 \% \pm 0.22 \%$.

488 The CH₄ emissions from natural gas will exacerbate climate warming. Calculated flux results
489 showed that the contribution of CH₄ to climate warming on a century and 20-year scale can reach
490 as high as 8.37 % and 23.17 % of CO₂, respectively. On the basis of predicted energy report and
491 calculated leakage rate, it is roughly predicted that natural gas leakage will delay China's realization
492 of carbon neutrality, which necessitates urgent attention to mitigate associated climate effects.
493 Future work should prioritize the development of more granular, bottom-up inventories based on

494 province-level activity data and infrastructure surveys to achieve a more accurate and robust
495 assessment of China's overall natural gas leakage.

496 **SUPPORTING INFORMATION**

497 Details about the Beijing Meteorological Tower, eddy observation system and navigation
498 observation station, daily summer variation in CO₂ flux from 2009 to 2017, total consumption,
499 electricity inflow and the proportion of natural gas in total energy consumption from 2013-2022,
500 spatial distribution of CO₂ and CH₄ fluxes with wind speed and direction, grid distribution of natural
501 gas consumption in Beijing, calculation methods of the flux source area and natural gas leakage rate,
502 uncertainty analysis of flux calculation, estimation of non-natural gas sources

503 **ACKNOWLEDGMENTS**

504 This work was supported by the National Key R&D Program of China (2023YFC3706103), the
505 Strategic Priority Research Program of the Chinese Academy of Sciences (XDB0760200), the
506 Beijing Municipal Natural Science Foundation (No. 8222075), the Youth Cross Team Scientific
507 Research Project of the Chinese Academy of Sciences (No. JCTD-2021-10) and the S&T Program
508 of Hebei (22373903D).

509 **DATA AVAILABILITY**

510 All the data generated or analyzed in this study are included in the published article and are available
511 from the authors upon reasonable request.

512 **AUTHOR CONTRIBUTION**

513 Haoyuan Chen: Formal analysis, methodology, data curation, visualization, and writing—original
514 draft; Tao Song: methodology and review; Yinghong Wang: methodology and review; Mengtian
515 Cheng: review; Kai Wang: data curation and review; Fuxin Liu: review; Xiaodong Chen: data
516 curation and review; Baoxian Liu: data curation and review; Guiqian Tang: supervision, project
517 administration, funding acquisition, writing—review and editing, and conceptualization; Yuesi
518 Wang: data curation and review.

519 **COMPETING INTERESTS**

520 The authors declare that they have no competing interests.

521 **REFERENCES**

522 Ars, S., Vogel, F., Arrowsmith, C., Heerah, S., Knuckey, E., Lavoie, J., Lee, C., Pak, N. M., Phillips,
523 J. L., and Wunch, D.: Investigation of the Spatial Distribution of Methane Sources in the

568 Helfter, C., Tremper, A. H., Halios, C. H., Kotthaus, S., Bjorkegren, A., Grimmond, C. S. B., Barlow,
569 J. F., and Nemitz, E.: Spatial and temporal variability of urban fluxes of methane, carbon
570 monoxide and carbon dioxide above London, UK, *Atmos. Chem. Phys.*, 16, 10543-10557,
571 <http://doi.org/10.5194/acp-16-10543-2016>, 2016.

572 Hu, W., Qin, K., Lu, F., Li, D., and Cohen, J. B.: Merging TROPOMI and eddy covariance
573 observations to quantify 5-years of daily CH₄ emissions over coal-mine dominated region, *Int.*
574 *J. Coal Sci. Technol.*, 11, 56, <https://doi.org/10.1007/s40789-024-00700-1>, 2024.

575 Hurry, J., Risk, D., Lavoie, M., Brooks, B.-G., Phillips, C. L., and Göckede, M.: Atmospheric
576 monitoring and detection of fugitive emissions for Enhanced Oil Recovery, *Int. J. Greenh. Gas*
577 *Con.*, 45, 1-8, <http://doi.org/10.1016/j.ijggc.2015.11.031>, 2016.

578 Kaimal, J. C., and Finnigan, J. J.: Atmospheric boundary layer flows: their structure and
579 measurement. New York: Oxford University Press, 1994.

580 Kaimal, J. C., Wyngaard, J. C., Izumi, Y., and Coté, O. R.: Spectral characteristics of surface-layer
581 turbulence, *Quart. J. R. Met. Soc.*, 98, 563-589, <http://doi.org/10.1002/qj.49709841707>, 1972.

582 Kemfert, C., Präger, F., Brauner, I., Hoffart, F. M., and Brauers, H.: The expansion of natural gas
583 infrastructure puts energy transitions at risk, *Nature Energy*, 7, 582-587,
584 <http://doi.org/10.1038/s41560-022-01060-3>, 2022.

585 Kljun, N., Calanca, P., Rotach, M. W., and Schmid, H. P.: A Simple Parameterisation for Flux
586 Footprint Predictions, *Boundary-Layer Meteorology*, 112, 503-523,
587 <http://doi.org/10.1023/b:Boun.0000030653.71031.96>, 2004.

588 Lamb, B. K., McManus, J. B., Shorter, J. H., Kolb, C. E., Mosher, B., Harriss, R. C., Allwine, E.,
589 Blaha, D., Howard, T., Guenther, A., Lott, R. A., Siverson, R., Westburg, H., and Zimmerman,
590 P.: Development of atmospheric tracer methods to measure methane emissions from natural
591 gas facilities and urban areas, *Environ. Sci. Technol.*, 29, 1468-1479,
592 <http://doi.org/10.1021/es00006a007>, 1995.

593 Lee, X.: Handbook of micrometeorology: A Guide for surface Flux Measurement and Analysis.
594 New York: Klewer Academic Publishers, 2004.

595 Li, X., Cohen, J. B., Tiwari, P., Wu, L., Wang, S., He, Q., Yang, H., and Qin, K.: Space-based
596 inversion reveals underestimated carbon monoxide emissions over Shanxi, *Commun. Earth*
597 *Environ.*, 6, 357, <https://doi.org/10.1038/s43247-025-02301-5>, 2025.

598 Liu, H. Z., Feng, J. W., Järvi, L., and Vesala, T.: Four-year (2006–2009) eddy covariance
599 measurements of CO₂ flux over an urban area in Beijing, *Atmos. Chem. Phys.*, 12, 7881-7892,
600 <http://doi.org/10.5194/acp-12-7881-2012>, 2012.

601 Liu, S., Liu, K., Wang, K., Chen, X., and Wu, K.: Fossil-Fuel and Food Systems Equally Dominate
602 Anthropogenic Methane Emissions in China, *Environ. Sci. Technol.*, 57, 2495-2505,
603 <http://doi.org/10.1021/acs.est.2c07933>, 2023.

604 Liu, Z., Liu, Z., Song, T., Gao, W., Wang, Y., Wang, L., Hu, B., Xin, J., and Wang, Y.: Long-term
605 variation in CO₂ emissions with implications for the interannual trend in PM(2.5) over the last
606 decade in Beijing, China, *Environ. Pollut.*, 266, 115014,
607 <http://doi.org/10.1016/j.envpol.2020.115014>, 2020.

608 Lu, F., Qin, K., Cohen, J. B., He, Q., Tiwari, P., Hu, W., Ye, C., Shan, Y., Xu, Q., Wang, S., and Tu,
609 Q.: Surface-observation-constrained high-frequency coal mine methane emissions in Shanxi,
610 China, reveal more emissions than inventories, consistent with satellite inversion, *Atmos.*

611 Chem. Phys., 25, 5837-5856, <https://doi.org/10.5194/acp-25-5837-2025>, 2025.

612 Mauder, M., and Foken, T.: Documentation and Instruction Manual of the Eddy Covariance
613 Software Package TK2, Proc. R. Soc. Med., 26, 42-46, <http://doi.org/10.5281/zenodo.20349>,
614 2004.

615 Moncrieff, J. B., Malhi, Y., and Leuning, R.: The propagation of errors in long-term measurements
616 of land - atmosphere fluxes of carbon and water, Global Change Biology, 2, 231-240,
617 <http://doi.org/10.1111/j.1365-2486.1996.tb00075.x>, 1996.

618 Pawlak, W., and Fortuniak, K.: Eddy covariance measurements of the net turbulent methane flux in
619 the city centre – results of 2-year campaign in Łódź, Poland, Atmos. Chem. Phys., 16, 8281-
620 8294, <http://doi.org/10.5194/acp-16-8281-2016>, 2016.

621 Pu, W., Sheng, J., Tian, P., Huang, M., Liu, X., Collett Jr, J.L., Li, Z., Zhao, X., He, D., Dong, F.:
622 On-road mobile mapping of spatial variations and source contributions of ammonia in Beijing,
623 China, Sci. Total Environ., 864, 160869, 2023.

624 Qin, K., Hu, W., He, Q., Lu, F., and Cohen, J. B.: Individual coal mine methane emissions constrained
625 by eddy covariance measurements: low bias and missing sources, Atmos. Chem. Phys., 24, 3009-
626 3028, <https://doi.org/10.5194/acp-24-3009-2024>, 2024.

627 Sargent, M. R., Floerchinger, C., McKain, K., Budney, J., Gottlieb, E. W., Hutyra, L. R., Rudek, J.,
628 and Wofsy, S. C.: Majority of US urban natural gas emissions unaccounted for in inventories,
629 Proc. Natl. Acad. Sci. U. S. A., 118, e2105804118, <http://doi.org/10.1073/pnas.2105804118>,
630 2021.

631 Schiferl, L.D., Hallward-Driemeier, A., Zhao, Y., Toledo-Crow, R., and Commane, R.: Missing
632 wintertime methane emissions from New York City related to combustion, EGUsphere, 2025,
633 1-28, <https://doi.org/10.5194/egusphere-2025-345>, 2025.

634 Seneviratne, S. I., Rogelj, J., Seferian, R., Wartenburger, R., Allen, M. R., Cain, M., Millar, R. J.,
635 Ebi, K. L., Ellis, N., Hoegh-Guldberg, O., Payne, A. J., Schleussner, C. F., Tschakert, P., and
636 Warren, R. F.: The many possible climates from the Paris Agreement's aim of 1.5 degrees C
637 warming, Nature, 558, 41-49, <http://doi.org/10.1038/s41586-018-0181-4>, 2018.

638 Shen, L., Jacob, D. J., Gautam, R., Omara, M., Scarpelli, T. R., Lorente, A., Zavala-Araiza, D., Lu,
639 X., Chen, Z., and Lin, J.: National quantifications of methane emissions from fuel exploitation
640 using high resolution inversions of satellite observations, Nat. Commun., 14, 4948,
641 <http://doi.org/10.1038/s41467-023-40671-6>, 2023.

642 Sherwin, E. D., Rutherford, J. S., Zhang, Z., Chen, Y., Wetherley, E. B., Yakovlev, P. V., Berman, E.
643 S. F., Jones, B. B., Cusworth, D. H., Thorpe, A. K., Ayasse, A. K., Duren, R. M., and Brandt,
644 A. R.: US oil and gas system emissions from nearly one million aerial site measurements,
645 Nature, 627, 328-334, <http://doi.org/10.1038/s41586-024-07117-5>, 2024.

646 Sun, W., Deng, L., Wu, G., Wu, L., Han, P., Miao, Y., and Yao, B.: Atmospheric Monitoring of
647 Methane in Beijing Using a Mobile Observatory, Atmosphere, 10, 554,
648 <http://doi.org/10.3390/atmos10090554>, 2019.

649 Vickers, D., and Mahrt, L.: Quality Control and Flux Sampling Problems for Tower and Aircraft
650 Data, J. Atmos. Oceanic Technol., 14, 512-526, [http://doi.org/10.1175/1520-0426\(1997\)014<0512:Qcafsp>2.0.Co;2](http://doi.org/10.1175/1520-0426(1997)014<0512:Qcafsp>2.0.Co;2), 1997.

651 Wang, P., Zhou, W., Xiong, X., Wu, S., Niu, Z., Cheng, P., Du, H., and Hou, Y.: Stable carbon
652 isotopic characteristics of fossil fuels in China, Sci. Total. Environ., 805, 150240,
653 <http://doi.org/10.1016/j.scitotenv.2021.150240>, 2022.

655 Wang, P., Zhou, W., Xiong, X., Wu, S., Niu, Z., Yu, Y., Liu, J., Feng, T., Cheng, P., Du, H., Lu, X.,
656 Chen, N., and Hou, Y.: Source Attribution of Atmospheric CO₂ Using ¹⁴C and ¹³C as Tracers
657 in Two Chinese Megacities During Winter, *JGR: Atmospheres*, 127, e2022JD036504,
658 <http://doi.org/10.1029/2022jd036504>, 2022.

659 Wang, Y., Guo, C. H., Chen, X. J., Jia, L. Q., Guo, X. N., Chen, R. S., and Wang, H. D.: Global
660 climate governance strategies and prospects for China's carbon neutrality path. *Forecasting
661 And Prospects Research Report*, 2021.

662 Webb, E. K., Pearman, G. I., and Leuning, R.: Correction of flux measurements for density effects
663 due to heat and water vapour transfer, *Q. J. R. Meteorolog. Soc.*, 106, 85-100,
664 <http://doi.org/10.1002/qj.49710644707>, 2007.

665 Weller, Z. D., Roscioli, J. R., Daube, W. C., Lamb, B. K., Ferrara, T. W., Brewer, P. E., and von
666 Fischer, J. C.: Vehicle-Based Methane Surveys for Finding Natural Gas Leaks and Estimating
667 Their Size: Validation and Uncertainty, *Environ. Sci. Technol.*, 52, 11922-11930,
668 <http://doi.org/10.1021/acs.est.8b03135>, 2018.

669 Weller, Z. D., Yang, D. K., and von Fischer, J. C.: An open source algorithm to detect natural gas
670 leaks from mobile methane survey data, *PLoS One*, 14, e0212287,
671 <http://doi.org/10.1371/journal.pone.0212287>, 2019.

672 Wunch, D., Toon, G. C., Hedenius, J. K., Vizenor, N., Roehl, C. M., Saad, K. M., Blavier, J.-F. L.,
673 Blake, D. R., and Wennberg, P. O.: Quantifying the loss of processed natural gas within
674 California's South Coast Air Basin using long-term measurements of ethane and methane,
675 *Atmos. Chem. Phys.*, 16, 14091-14105, <http://doi.org/10.5194/acp-16-14091-2016>, 2016.

676 Zheng, B., Cohen, J. B., Lu, L., Hu, W., Tiwari, P., Lolli, S., Garzelli, A., Su, H., and Qin, K.: How
677 can we trust TROPOMI based Methane Emissions Estimation: Calculating Emissions over
678 Unidentified Source Regions, *EGUsphere [preprint]*, <https://doi.org/10.5194/egusphere-2025-1446>, 2025.

679

680 Zöll, U., Brümmer, C., Schrader, F., Ammann, C., Ibrom, A., Flechard, C. R., Nelson, D. D.,
681 Zahniser, M., and Kutsch, W. L.: Surface-atmosphere exchange of ammonia over peatland
682 using QCL-based eddy-covariance measurements and inferential modeling, *Atmos. Chem.
683 Phys.*, 16, 11283-11299, <http://doi.org/10.5194/acp-16-11283-2016>, 2016.

684